Precision measurement based on ultracold atoms and cold molecules

Jun Ye, Sebastian Blatt, Martin M. Boyd, Seth M. Foreman, Eric R. Hudson, Tetsuya Ido, Benjamin Lev, Andrew D. Ludlow, Brian C. Sawyer, Benjamin Stuhl, Tanya Zelevinsky

JILA, National Institute of Standards and Technology and University of Colorado
Department of Physics, Univeristy of Colorado, Boulder, CO 80309-0440, USA
Ye@jila.colorado.edu, Web: http://jilawww.colorado.edu/YeLabs

Abstract. Ultracold atoms and molecules provide ideal stages for precision tests of fundamental physics. With microkelvin neutral strontium atoms confined in an optical lattice, we have achieved a fractional resolution of 4×10^{-15} on the $^1S_0 - {}^3P_0$ doubly-forbidden ^{87}Sr clock transition at 698 nm. The overall systematic uncertainty of the clock is evaluated below the 10^{-15} level. The ultrahigh spectral resolution permits resolving the nuclear spin states of the clock transition at small magnetic fields, leading to measurements of the $^3P_0$ magnetic moment and metastable lifetime. In addition, photoassociation spectroscopy performed on the narrow $^1S_0 - {}^3P_1$ transition of ^{88}Sr shows promise for efficient optical tuning of the ground state scattering length and production of ultracold ground-state molecules. Lattice-confined Sr_2 molecules are suitable for constraining the time-variation of electron-proton mass ratio. In a separate experiment, cold, ground state polar molecules produced from Stark decelerators have enabled an order of magnitude improvement in measurement precision of ground-state, Λ-doublet microwave transitions in the OH molecule. Comparing the laboratory results to those from OH megamasers in interstellar space will allow a sensitivity of 10^{-6} for measuring the potential time variation of the fundamental fine structure constant $\Delta\alpha/\alpha$ over 10^{10} years. These results have also led to improved understandings in the molecular structure. The study of the low magnetic field behavior of OH in its $^2\Pi_{3/2}$ ro-vibronic ground state precisely determines a differential Landé g-factor between opposite parity components of the Λ-doublet.

INTRODUCTION

The unique atomic structure of alkaline earth atoms such as strontium permits studies of narrow line physics based on the forbidden $^1S_0 - {}^3P_0$ and $^1S_0 - {}^3P_1$ transitions. The millihertz-wide $^1S_0 - {}^3P_0$ ^{87}Sr line at 698 nm is especially attractive for an optical atomic clock. Using optically cooled ^{87}Sr atoms in a zero-Stark-shift, one dimensional optical lattice and an ultrastable probe laser with sub-Hz line width, we have achieved repeatable Fourier-limited linewidths of below 2 Hz. This represents a fractional resolution of $\sim 4 \times 10^{-15}$. We have characterized the systematic uncertainty of the clock $< 1 \times 10^{-15}$.

The hertz level linewidths allowed us to resolve all hyperfine components of the clock transition (nuclear spin is $I = 9/2$ for ^{87}Sr), and measure the differential ground-excited g-factor that arises from hyperfine mixing of $^3P_0$ with $^3P_1$ and $^1P_1$. This measurement yielded an experimental determination of the $^3P_0$ lifetime.

We have also carried out narrow line photoassociation studies with ^{88}Sr near the $^1S_0 - ^3P_1$ dissociation limit. The 15 kHz natural width of the molecular line allowed observation of nine least-bound molecular states. The line shapes were sensitive to thermal effects even at $2\,\mu$K ultracold temperatures and to zero-point shifts by the optical lattice confinement. The combination of a narrow width of the least-bound state and its strong coupling to the scattering state should allow efficient tuning of the ground state scattering length with the optical Feshbach resonance technique. We also predict that the deepest-bound level we observed decays to a single ground electronic molecular state with 90% efficiency. This is promising for producing ultracold stable molecules.

Substantial progress is made recently [1, 2, 3, 4] in the control of molecular degrees of freedom, with the goal of preparing molecules in a single quantum state for both internal and external degrees of freedom. Cold molecules provide a new paradigm for precision tests of possible time-variations of fundamental constants. For example, when both electronic and vibrational transitions are probed precisely, one would be comparing clocks built from two fundamentally different interactions, one of the origin of quantum electrodynamics (α), the other of strong interaction (electron/proton mass ratio β).

In our laboratory we have demonstrated Stark deceleration of both hydroxyl radicals (OH) and formaldehyde (H_2CO) molecules to near rest [3, 5]. A supersonic beam of OH can be accelerated/decelerated to a mean speed adjustable between 550 m/s to rest, with a translational temperature tunable from 1 mK to 1 K. These velocity-manipulated stable "bunches" contain 10^4 to 10^6 molecules at a density of 10^5 to 10^7 cm^{-3} and they are ideal for high resolution microwave spectroscopy using Rabi or Ramsey techniques. The entire manifold of the astrophysically important $J = 3/2$ Λ-doublet [6, 7], including both the main lines (ΔF $= 0$) and the magnetically sensitive satellite-lines (ΔF $= \pm1$), are measured with a ten-fold accuracy improvement, leading to the refinement of the theory of angular momentum couplings in OH. These measurements highlight the ability of cold molecules not only to enhance our understanding of unexplored regimes of molecular coupling, but also to contribute toward searches of non-Standard Model physics, e.g. the variation of fundamental constants such as α and β, which may be measured by comparing Earth-bound OH with that found in OH megamasers [8, 9, 10].

OPTICAL ATOMIC CLOCK

Optical clocks based on neutral atoms tightly confined in optical lattices have recently begun to show promise as future time/frequency standards [11, 12, 13, 14]. These optical lattice clocks enjoy a high signal-to-noise ratio from the large numbers of atoms, while at the same time allowing Doppler-free interrogation of the clock transitions for long probing times, a feature typically associated with single trapped ions. Currently, detailed evaluations of systematic effects for the $^1S_0 - ^3P_0$ sub-Hz line in ^{87}Sr are being performed in several independent systems [11, 14, 15]. Here we present our recent progress in evaluation of systematic effects below the 10^{-15} level. These measurements have greatly benefited from an ultranarrow spectral linewidth corresponding to a line quality factor $Q \sim 2.4 \times 10^{14}$ [16].

EXPERIMENTAL TECHNIQUE Neutral strontium atoms are loaded into a dual-stage magneto-optical trap, where they are first cooled to mK temperatures using the

strong (32 MHz) $^1S_0 - {}^1P_1$ line and then to μK temperatures using the weak (7 kHz) $^1S_0 - {}^3P_1$ intercombination line [17]. Approximately 10^4 atoms are loaded into a 1D $\sim$300 mW standing-wave optical lattice. The lattice wavelength of 813 nm is chosen to zero the net Stark shift of the clock transition [18], thus also eliminating line broadening due to the trapping potential inhomogeneity. The atoms are confined in the Lamb-Dicke regime, such that the recoil frequency (5 kHz) is much smaller than the axial trap frequency (50 kHz). The probe is carefully aligned along the lattice axis and spectroscopy is both Doppler-free and recoil-free. In the transverse direction, the lattice provides a trapping frequency of about 150 Hz, which is smaller than the recoil frequency, but still much larger than the clock transition linewidth. Atoms can be held in the perturbation-free lattice for times exceeding 1 s, which is important for Hz-level spectroscopy.

We probe the extremely narrow natural linewidth (1 mHz) of the clock transition in ^{87}Sr with a cavity-stabilized diode laser operating at 698 nm. The high finesse cavity is mounted in a vertical orientation to reduce sensitivity to vibrations [19]. To characterize the probe laser, we compare it to a second stable laser locked to an identical cavity. This comparison shows laser linewidths below 0.2 Hz for a 3 s integration time (resolution-limited) and $\sim$2.1 Hz for a 30-s integration time (limited by nonlinear laser drift).

For absolute frequency measurements of the clock transition, we frequency count the probe laser against a hydrogen maser signal calibrated by the NIST primary Cs fountain clock. A self-referenced octave spanning frequency comb [20] is locked to the probe laser and its repetition rate is counted. The instability of this frequency counting signal is $2.5 \times 10^{-13} \tau^{-1/2}$, where τ is the integration time. This is the limitation on our statistics. The clock frequency is 429,228,004,229,876(4.5) Hz, limited by the maser transfer.

SYSTEMATIC EFFECTS When the Zeeman sublevels of the ground and excited clock states are degenerate (nuclear spin $I = 9/2$ for $^1S_0$, $^3P_0$), linewidths of < 5 Hz ($Q \sim 10^{14}$) are achieved. This spectral resolution greatly facilitates evaluation of systematic effects below the 10^{-15} level. The differential magnetic moment between the ground and excited states leads to a first-order Zeeman shift of the clock transition. This can lead to shifts or broadening from stray magnetic fields, depending on the population distribution among the magnetic sublevels. By varying the strength of an applied magnetic field in three orthogonal directions and measuring the spectral linewidth as a function of field strength, the uncertainty of the residual magnetic field has been reduced to < 5 mG for each axis. The resulting net uncertainty for magnetically-induced frequency shifts is now <0.2 Hz ($<5 \times 10^{-16}$). Understanding and controlling the magnetic shifts is essential for the ^{87}Sr optical clock since the accuracy of all recent measurements has been limited by the sensitivity to magnetic fields [12, 11, 14].

Reduction of other systematic uncertainties (due to lattice intensity, probe intensity, and atom density) is straightforward with our high spectral resolution. Recent results in JILA indicate an overall systematic uncertainty below 1×10^{-15} for the Sr lattice clock. Recently we have stabilized the microwave phase of the fiber that transmits the maser reference from NIST to JILA to preserve the full accuracy of the microwave reference, the averaging times necessary to achieve 10^{-15} uncertainties for all systematic effects are still long. Our approach to studying most systematic effects is thus to make frequency measurements under several values of the same systematic parameter within a time interval sufficiently short that the mode frequency of the ultrastable optical cavity
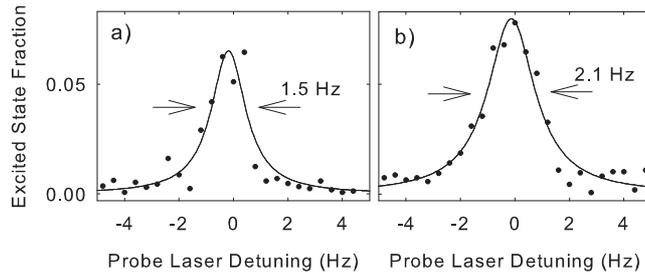
FIGURE 1. Typical spectra of the $^1S_1 - ^3P_0$ clock transition, exhibiting a line quality factor $Q \sim 2.4 \times 10^{14}$. The linewidths are a) 1.5(2) Hz and b) 2.1(2) Hz, in good agreement with the probe time limit of 1.8 Hz. One such trace takes approximately 30 seconds to collect (since the atom trap must be reloaded for each data point), and involves no averaging or normalization.
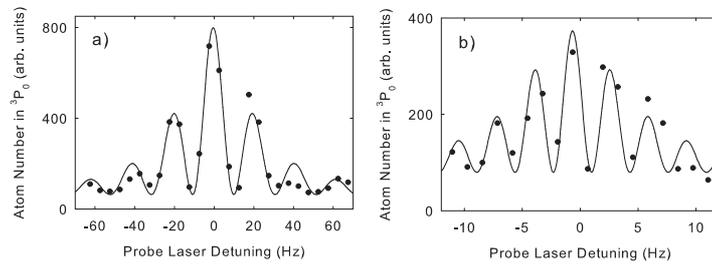

FIGURE 2. Ramsey spectra of the $^1S_1 - ^3P_0$ clock transition. a) The preparation and probe pulses are 20 ms, the evolution time is 25 ms. Fringe width is 10.4(2) Hz. b) The preparation and probe pulses are 80 ms, the evolution time is 200 ms. Fringe width is 1.7(1) Hz.

used as a reference does not drift over the desired level of uncertainty. In addition, we have locked the probe laser to the clock transition with the goal of directly comparing the Sr clock to the Hg$^+$ and Al$^+$ optical atomic clocks at NIST.

HIGH SPECTRAL RESOLUTION The recent improvements to the probe laser stabilization have allowed us to probe the clock transition at an unprecedented level of spectral resolution. With the nuclear spin degeneracy removed by a small magnetic field, individual transition components allow exploring the ultimate limit of our resolution by eliminating any broadening due to residual magnetic fields or light shifts. Figure 1 shows sample spectra of the $^1S_0(m_F = 5/2) - ^3P_0(m_F = 5/2)$ transition, where m_F is the nuclear spin projection onto the lattice polarization axis. The linewidths are probe time limited to ~ 1.8 Hz, representing a line Q of $\sim 2.4 \times 10^{14}$. This Q value is reproduced reliably, with some scatter of the measured linewidths in the $\sim 1 - 3$ Hz range.

Besides the single-pulse spectroscopy of the clock line, two-pulse optical Ramsey experiments were also performed on an isolated Zeeman component. When a system is limited by the atom or trap lifetime, the Ramsey technique can yield higher spectral resolution at the expense of signal contrast. An additional motivation for Ramsey spectroscopy in the Lamb-Dicke regime is the ability to use long interrogation pulses, which results in a drastically narrowed Rabi pedestal compared to free-space atoms. The reduced number of Ramsey fringes facilitates the identification of the central fringe.
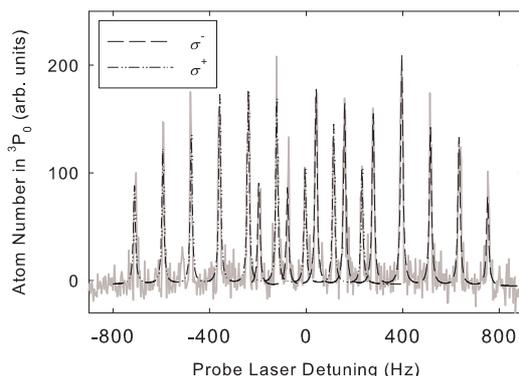
FIGURE 3. Clock transition with resolved nuclear spin sublevels. The probe light is polarized perpendicular to the magnetic field direction and lattice polarization, in order to probe σ transitions. The σ^+ and σ^- components are seen as two combs with nine individual lines (nuclear spin $I = 9/2$). The spacing between these lines is determined by the differential g-factor of the two clock states, Δg.

Figure 2(a) shows a sample Ramsey spectrum, where the preparation and probe pulses are 20 ms and the free evolution time is 25 ms, yielding a pattern with a fringe width of 10.4(2) Hz, as expected. Figure 2(b) shows the same transition with the preparation and probe pulses of 80 ms and the evolution time of 200 ms. Here the width of the central fringe is reduced to 1.7(1) Hz. Both spectra exhibit no degradation of the fringe contrast. However, the quality of the spectra deteriorated at longer evolution times. Our inability to increase the resolution as compared to single-pulse Rabi spectroscopy suggests that the linewidth is not limited by the atom or trap lifetime, but rather by phase decoherence between the light and atoms, most likely due to nonlinear laser frequency fluctuations during the scan. This is supported by Rabi spectroscopy where the the laser stability appeared to limit the linewidth repeatability at the probe time limit near 0.9 Hz.

MAGNETIC MOMENT AND LIFETIME MEASUREMENTS This high spectral resolution allowed us to perform NMR-type experiments in the optical domain. We applied a small magnetic bias field and made direct observations of the magnetic sublevels associated with the nuclear spin. The magnetic moments of $^1S_0$ and $^3P_0$ differ because of hyperfine-induced state mixing of $^3P_0$ with $^3P_1$ and $^1P_1$. The differential Landé g-factor, Δg, leads to a ~ 110 Hz/(G m_F) linear Zeeman shift of the clock line. This Zeeman shift measurement is also a direct determination of the perturbed wavefunction of $^3P_0$, and hence of its metastable (~ 100 s) lifetime. Our approach uses only a small magnetic field, while traditional NMR experiments performed on either $^1S_0$ or $^3P_0$ would need large magnetic fields to induce splitting in the radio frequency range. As larger fields can give rise to additional field-induced state mixing between $^3P_0$, $^3P_1$, and $^1P_1$ (we estimate that a field as weak as 16 G causes a 1% change in Δg), the use of a small field permits an accurate, unperturbed measurement of mixing effects. Additionally, this measurement on the resolved transitions is helpful for the optical clock accuracy evaluation, as one can look for changes in the splitting as a function of the lattice polarization to measure the effect of polarization-dependent light shifts.

The differential nuclear magnetic moment can be determined by setting the probe

light polarization parallel to the lattice polarization axis and magnetic field direction, and fitting the resulting Zeeman splitting of the π-transitions. However, such a measurement requires an independent calibration of the magnetic field in the trap region, and is sensitive to the linear drift of the probe laser during the scan, which manifests as a fictitious magnetic field. In a more powerful measurement scheme, we polarize the probe laser perpendicular to the quantum axis to excite σ^+ and σ^- transitions, and we obtain spectra as in Fig. 3. Each spectrum yields information about the Δg value from the splitting between the neighboring σ^+ or σ^- lines and about the magnetic field from the splitting between the two manifolds, since the ground state magnetic moment is well known [21]. Thus, the nuclear spin is used as a magnetometer. Since the field calibration and the Δg measurements are done simultaneously, this approach is immune to any linear laser drift or magnetic field variation. This method also eliminates a Δg sign ambiguity that is present in the π-transition approach.

We found that the linear Zeeman shift of the clock transition is $-108.8(4)$ Hz/(G m_F), corresponding to a $^3P_0$ magnetic moment of $-1.735(6)\mu_N$, where μ_N is the nuclear magneton. To check for systematic errors related to light shifts, we varied the intensities of the lattice laser (by $> 50\%$) and the probe laser (by a factor of 10) and observed no statistically significant change in the measured splitting. We have also searched for possible m_F-dependent systematics by comparing the splitting frequency of different pairs of sublevels. The magnetic field was varied to verify the field independence of the measurement. A combination of our Δg measurements with atomic theory of hyperfine mixing [22, 23] can predict the metastable lifetime of $^3P_0$. Depending on the specifics of the chosen model, the predicted lifetimes range between 100 and 180 seconds. Although our experimental measurement error is small, it results in a relatively large model-dependent error associated with the lifetime measurement, which gives the value of 140(40) s. Still it is a very useful confirmation of recently calculated values [24, 25], since a direct and accurate measurement of the natural lifetime is difficult due to limitations from the trap lifetime and blackbody quenching.

NARROW LINE PHOTOASSOCIATION

While we worked with the doubly-forbidden transition of ^{87}Sr in the optical clock experiments, we used ^{88}Sr for cold collision studies. The even isotope is the most abundant (83%), and has a zero nuclear spin. The large abundance increases the sample density in the trap for more efficient collisions, and the absence of the nuclear spin greatly simplifies the molecular potentials, thus facilitating comparisons of experiment and theory. With ultracold ^{88}Sr in a zero-Stark-shift optical lattice (914 nm wavelength), we performed narrow line photoassociation (PA) spectroscopy near the $^1S_0 - ^3P_1$ intercombination transition [26]. Nine least-bound vibrational molecular levels associated with the long-range 0_u and 1_u excited molecular potentials were measured and identified. The measured PA resonance strengths showed that optical tuning of the ground state scattering length should be possible without significant atom loss. The calculated decay strengths of the photoassociated molecules to the ground electronic state indicate great promise for ultracold stable molecule production.

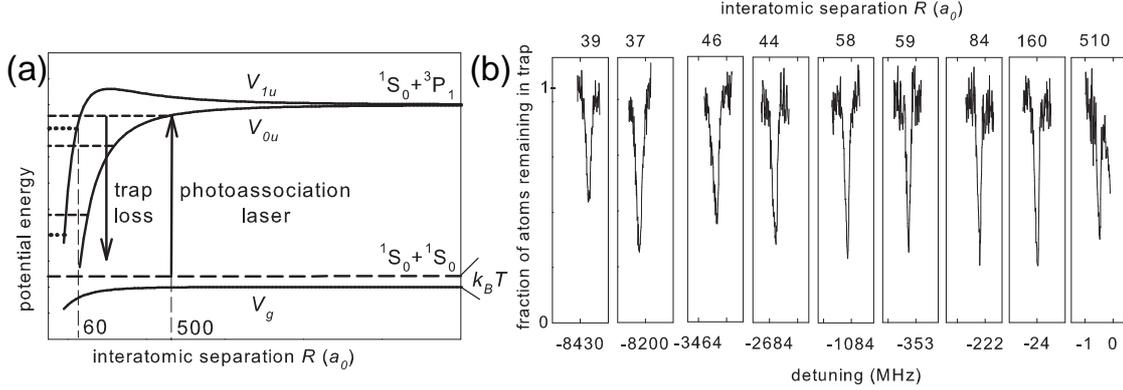In contrast to prior PA work that utilizes strongly allowed transitions with typical

FIGURE 4. (a) Schematic diagram of the long-range Sr_2 molecular potentials. The ground state has *gerade* symmetry and its energy is given by the potential V_g, while the excited state *ungerade* potentials that support transitions to the ground state are V_{0u} and V_{1u}. All vibrational states of 0_u and 1_u (dashed and dotted lines, respectively) are separated by more than the natural line width, permitting high resolution PA spectroscopy very close to the dissociation limit when the atoms are sufficiently cold. (b) The spectrum of the long-range Sr_2 molecule near the $^1S_0 - ^3P_1$ dissociation limit. The horizontal scale is marked on the rightmost panel and is the same for each of the nine blocks; different PA laser intensities were used for each line due to largely varying transition strengths. The top labels indicate the interatomic separations that correspond to the classical outer turning points of each resonance.

line widths in the MHz range, here the spin-forbidden atomic $^1S_0 - ^3P_1$ line has a natural width of ~ 7 kHz. This narrow width allows us to measure the least-bound vibrational levels that would otherwise be obscured by a broad atomic line, and to observe characteristic thermal line shapes even at μK atom temperatures. It also permits examination of the unique crossover regime between the van der Waals and resonant dipole-dipole interactions that occurs very close to the dissociation limit. This access to the van der Waals interactions ensures large bound-bound Franck-Condon factors, and may lead to more efficient creation of cold ground state Sr_2 molecules with two-color PA than what is possible using broad transitions.

Figure 4(a) illustrates the relevant potential energy curves for the Sr_2 dimer as a function of interatomic separation R. The photoassociation laser induces allowed transitions from the separated $^1S_0$ atom continuum at $T \sim 2$ μK to the bound vibrational levels of the excited potentials V_{0u} and V_{1u}, corresponding to the total atomic angular momentum projections onto the internuclear axis of 0 and 1, respectively. The long-range potentials are determined by the C_6/R^6 (van der Waals) and C_3/R^3 (resonant dipole-dipole) interactions. The values of the C_3 and C_6 coefficients are adjusted in the multi-channel theory model [27] so that bound states exist at the experimentally determined resonance energies. The C_3 coefficient can be expressed in terms of the atomic lifetime τ as $C_3 = 3\hbar c^3/(4\tau\omega^3)$, where $\hbar\omega$ is the transition energy and c is the speed of light. Our results yielded a C_3 coefficient that corresponds to the $^3P_1$ lifetime of 21.5(2) μs.

To trace out the molecular line spectra, a frequency-stabilized 689 nm diode laser is tuned near the $^1S_0 - ^3P_1$ intercombination line. The laser frequency is stepped, and after 320 ms of photoassociation at a fixed frequency the atoms are released from the optical lattice trap and counted by a strongly resonant light pulse. At a PA resonance, the atom number drops as excited molecules form and subsequently decay to ground state

molecules in high vibrational states or hot atoms that cannot remain trapped. Figure 4(b) shows the nine observed PA line spectra near the dissociation limit. The individual lines were fit to convolutions of a Lorentzian profile with an initial thermal distribution, and distinct thermal tails were observed even at the ultracold $\sim 1-3$ μK temperatures. In addition, the strong axial lattice confinement alters the collisional dynamics, and the two dimensional effects factor into the lineshapes as a larger density of states at small thermal energies, and as a red shift by the lattice zero-point confinement frequency.

Intercombination transitions of alkaline earths such as Sr are particularly good candidates for optical control of the ground state scattering length. These optical Feshbach resonances are of great interest for Sr, since magnetic Feshbach resonances are absent for the $^1S_0$ ground state, and the background scattering length is too small to allow evaporative cooling [28]. Using the -0.4 MHz PA line (see Fig. 4(b)) should allow tuning the ground state scattering length [29] by ± 300 a_0 (a_0 is the Bohr radius). In contrast, optical tuning of the scattering length in alkali ^{87}Rb [30] achieved tuning of ± 90 a_0 at much larger PA laser intensities. In addition, the Sr system will have a loss rate of [29] orders of magnitude smaller than the ^{87}Rb experiment. The overall efficiency gain of over 5 orders of magnitude is possible for Sr because the narrow intercombination transition allows access to the least-bound molecular state, and the PA line strength exponentially increases with decreasing detuning from the atomic resonance [29]. The above scattering length tunings and atom loss values accessible with the -0.4 MHz resonance result in the elastic and inelastic collision rates of $\sim$600/s and $\sim$0.1/s, respectively.

Narrow line PA is also suitable for efficient production of ultracold molecules in the ground electronic state. The bound-bound Franck-Condon factor calculations show that about 90% of the molecules photoassociated into the -8.4 GHz bound state decay to a single ground state vibrational level (distributed between only two rotational sublevels). Because the Sr excited state molecular potential is strongly influenced by van der Waals (C_6) interactions, the wavefunction overlap with the ground molecular bound states is large, making it possible to use low-power lasers in a Raman configuration to coherently transfer the molecules into the absolute ground ro-vibrational molecular state. Other exciting prospects include using the Raman scheme to perform precision measurements of the molecular ground state vibrational spacings with the goal of constraining temporal variations of the proton-electron mass ratio, and combining strontium with other alkaline earth atoms to create strongly interacting ultracold polar molecules in an optical lattice.

PRECISION MEASUREMENT BASED ON COLD OH MOLECULES

Comparison of different atomic clock systems [31] has provided tight constraints on the time variation of various fundamental constants, including α, during the modern epoch. However, observation of absorption lines in distant quasars [32, 33] provides conflicting results about possible α variation over cosmological time. Recently, there has been much interest in using OH megamasers in interstellar space to constrain the evolution of fundamental constants [8, 9, 10] with several key advantages. Most importantly, the multiple lines (that have different dependence on the fundamental constants) arising from one of these localized sources differentiate the relative Doppler shift from true
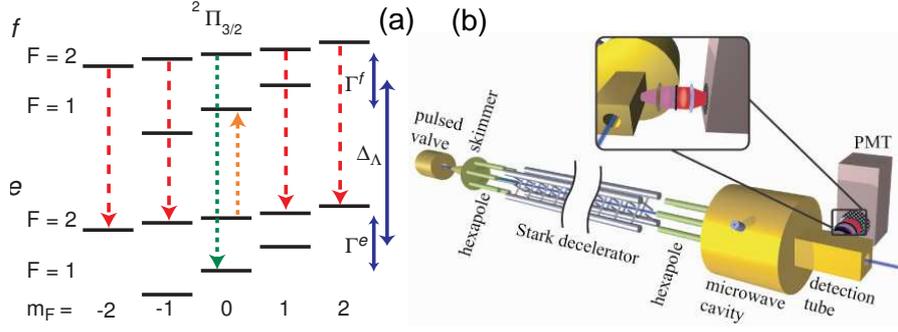
FIGURE 5. (a) OH ground Λ-doublet state. The arrows represent the transitions induced by the applied microwave pulses. Long-dashed arrows depict main-line π-transitions (ΔF=0) while short-dashed show measured satellite lines (ΔF=±1). (b) Schematic of experiment (inset depicts detection region).

variation in the transition frequency. Furthermore, it can been shown that the sum (Δ_Λ) and difference (Γ^f and Γ^e) of the $\Delta F = 0$ (F is total angular momentum) transition frequencies in the ground Λ-doublet of OH depend on α as $\alpha^{0.4}$ and α^4, respectively (see Fig. 5) [8]. Thus, by comparing these quantities as measured from OH megamasers to laboratory values, it is possible to remove the Doppler shift systematic and constrain α over cosmological time. Because of the unique properties of the Λ-doublet, the $\Delta F = 0$ transitions are extremely insensitive to magnetic fields, while the $\Delta F = \pm1$ satellite transitions can be used to calibrate the B-field. However, for the current limits on $\Delta\alpha/\alpha$ the change in the relevant measurable quantities is on the order of 100 Hz, which, prior to this work, was the accuracy of the best laboratory based measurement [37]. Moreover, an astrophysical measurement of OH megamasers, scheduled for later this year, expects a resolution better than 100 Hz [38], and thus better laboratory measurements of the OH Λ-doublet are imminently needed to allow for tighter constraints on $\Delta\alpha/\alpha$.

Experimentally, we focus on the electric dipole allowed, π (Δm_F=0) and σ (Δm_F=±1) transitions between the Λ-double parity states, as shown by arrows in Fig. 5(a). We write these states in the $|F, m_F, p\rangle$ basis and distinguish π-transitions from states by substituting Δp for the parity value, p. The hyperfine energies of the parity states are written as $\Gamma^{f,e} = \bar{\Gamma} \pm \xi/2$, where the average splitting, $\bar{\Gamma}$, and difference, ξ, are approximately 54.1 and 1.96 MHz, respectively [37]. Similarly, the g-factors are written $g^{f,e} = \bar{g} \pm \delta g/2$, where δg is 0.3% of $\bar{g}$ [36].

We utilize the Stark decelerator and microwave spectroscopy [6, 7] to obtain high spectral resolutions. In brief, the Stark decelerator provides OH primarily in the strongest, weak electric (E) field-seeking states, $|F, m_F, p\rangle = |2, \neq0, f\rangle$. Typical operation produces a 10^6 cm^{-3} dense packet with mean velocity controllable from 410 m/s down to nearly rest and a minimum temperature of 5 mK [3]. We choose to run the decelerator at 200 m/s as a compromise between slowing efficiency, microwave power, and interrogation time. We perform Rabi or Ramsey spectroscopy by interrogating the OH packet with one or more microwave pulses referenced to the Cs standard [6, 7]. Laser-induced fluorescence provides state detection by exciting the f manifold—equally driving the two hyperfine states—with 282 nm light and registering a fraction of the subsequent 313 nm emission with a photomultiplier tube. Main and satellite transitions

originating from $|2, m_F, f\rangle$ are driven with a single microwave pulse and detected by registering a reduction in photon counts (see Fig 5(a)).

The 10 cm long, TM_{010} microwave cavity is tuned near the $|2, m_F, \Delta p\rangle$ main line. A solenoid is wound around the cavity and encased in a μ-metal magnetic shield. The latter reduces the ambient field to $\leq$6 mG, while the former can apply a B-field >10 G along the resonant TM_{010} axis, which itself is aligned along the OH beam path. At the $|2, m_F, \Delta p\rangle$ frequency, the cavity E- and B-fields are nearly collinear—determined by the absence of observed σ-transitions—and the E-field magnitude is constant over 80% of the cavity. In contrast, the satellite-line frequencies are detuned far enough from cavity resonance to distort the associated intracavity E-field magnitude and direction, and we observe both π- ($\mathbf{E} \parallel \mathbf{B}$) and σ- ($\mathbf{E} \perp \mathbf{B}$) transitions on these lines.

We calibrate the intracavity B-field by tracking the $|2, m_F, f\rangle \rightarrow |1, m'_F, e\rangle$ satellite splitting as a function of B-field in the <1 G regime where the Zeeman theory is well-understood. Concurrent observation of the π- and σ-lines provides cross-checks on the B-field calibration. Their relative peak heights and frequency shifts versus cavity position also provide a tool for mapping E-field direction and power inhomogeneities. Under a residual B-field of <6 mG, the transition frequencies of the two main lines ($|2, m_f, f\rangle \rightarrow |2, m_f, e\rangle$ and $|1, m_f, f\rangle \rightarrow |1, m_f, e\rangle$) are measured to be (1 667 358 996 $\pm$ 4) Hz and (1 665 401 803 $\pm$ 12) Hz, respectively. These results are limited only by statistical uncertainties as other systematic shifts, such as from collisions, stray electric field, doppler shift, and black body radiation, are collectively <3 Hz [6]. When a bias B-field is applied to test the hyperfine structure theory, four peaks become visible for the $|2, m_f, f\rangle \rightarrow |2, m_f, e\rangle$ transition since for π-transitions $m_F = m'_F = 0$ is selection-rule forbidden. Precise measurements of transition frequencies of different m_F components under various B-field values determine $\bar{\delta} g_F = 1.267(5) \times 10^{-3}$, 1σ consistent with Radford measurements [36] in the J-basis at B = 0.6-0.9 T of $\delta g_J = 1.29(2) \times 10^{-3}$. Higher precision measurements in both regimes may distinguish a difference.

We have also measured the magnetically sensitive satellite-line transition frequencies. Specifically, we trace the $\nu_{21} = |2, 0, f\rangle \rightarrow |1, 0, e\rangle$ and $\nu_{12} = |2, 0, e\rangle \rightarrow |1, 0, f\rangle$ frequencies versus B-field. These Zeeman transitions are first-order insensitive to B-field, which suppresses spurious frequency shift contributions from calibration and ambient field uncertainties. Nearly overlapping π- and σ-transitions preclude an accurate measurement at zero applied field, and instead we must magnetically split the lines. The theory fit is used to project the data down to zero applied B-field. The uncertainty due to the ambient field on the line frequencies is estimated <0.6 Hz. Thus, $\nu_{21} = 1\,720\,529\,887(10)$ Hz. For the ν_{12} line, we use the distorted E-field at the cavity entrance to drive $|2, \pm 1, f\rangle \rightarrow |2, 0, e\rangle$ σ-transitions. A second microwave pulse then drives the π-transition to $|1, 0, f\rangle$. We measure $\nu_{12} = 1\,612\,230\,825(15)$ Hz. These values provide a tenfold improvement over the previous measurement accuracy [37].

Variation of α may be constrained by taking the sum and difference of either the main- or satellite-lines. The difference is sensitive to α while the sum measures the red-shift systematic. The satellite-lines offer a 55-fold increase in resolution over the main-lines due to the $2\bar{\Gamma}$ versus ξ separation [8]. Now that the complete Λ-doublet is measured with high-precision, one can simultaneously constrain variation of α and β [9]. All four lines must be detected from the same source, and the closure criterion, i.e., the zero difference of the averages of the main- and satellite-line frequencies, provides a

critical systematics check. We obtain an Earth-bound closure of 44±21 Hz. Imminent astrophysical measurements of the satellite-lines below the 100 Hz level [38] highlight the prescience of our study for observing the variation of fundamental constants.

ACKNOWLEDGMENTS

REFERENCES

1. J. Weinstein *et al.*, Nature **395**, 148 (1998).
2. H. L. Bethlem *et al.*, Phys. Rev. Lett. **83**, 1558 (1999).
3. J. Bochinski *et al.*, Phys. Rev. Lett. **91**, 243001 (2003).
4. J. Sage *et al.*, Phys. Rev. Lett. **94**, 203001 (2005).
5. E. R. Hudson *et al.*, Phys. Rev. A **73**, 063404 (2006).
6. E. R. Hudson *et al.*, Phys. Rev. Lett. **96**, 143004 (2006).
7. B. Lev *et al.*, arXiv:physics/0608194 (2006).
8. J. Darling, Phys. Rev. Lett. **91**, 011301 (2003).
9. J. Chengalur and N. Kanekar, Phys. Rev. Lett. **91**, 241302 (2003).
10. N. Kanekar *et al.*, Phys. Rev. Lett. **95**, 261301 (2005).
11. A. Ludlow *et al.*, Phys. Rev. Lett. **96**, 033003 (2006).
12. M. Takamoto *et al.*, Nature **435**, 321 (2005).
13. Z. Barber *et al.*, Phys. Rev. Lett. **96**, 083002 (2006).
14. A. Brusch *et al.*, Phys. Rev. Lett. **96**, 103003 (2006).
15. M. Takamoto *et al.*, physics/0608212 (2006).
16. M. Boyd *et al.*, to be published (2006).
17. T. Loftus *et al.*, Phys. Rev. A **70**, 063413 (2004).
18. T. Ido and H. Katori, Phys. Rev. Lett. **91**, 053001 (2003).
19. M. Notcutt *et al.*, Opt. Lett. **30**, 1815 (2005).
20. T. Fortier *et al.*, Opt. Lett. **28**, 2198 (2003).
21. L. Olschewski, Zeitschrift für Physik **249**, 205 (1972).
22. H. Kluge and H. Sauter, Zeitschrift für Physik **270**, 295 (1974).
23. B. Lahaye and J. Margerie, Journal de Physique **36**, 943 (1975).
24. S. Porsev and A. Derevianko, Phys. Rev. A **69**, 042506 (2004).
25. R. Santra *et al.*, Phys. Rev. A **69**, 042510 (2004).
26. T. Zelevinsky *et al.*, Phys. Rev. Lett. **96**, 203201 (2006).
27. R. Ciuryło *et al.*, Phys. Rev. A **70**, 062710 (2004).
28. P. Mickelson *et al.*, Phys. Rev. Lett. **95**, 223002 (2005).
29. R. Ciuryło *et al.*, Phys. Rev. A **71**, 030701(R) (2005).
30. M. Theis *et al.*, Phys. Rev. Lett. **93**, 123001 (2004).
31. E. Peik, *et al.*, Phys. Rev. Lett. **93**, 170801 (2004).
32. J. K. Webb, *et al.*, Phys. Rev. Lett. **87**, 091301 (2001).
33. R. Quast, D. Reimers, and S. Levshakov, Astron. Astrophys. **415**, L7 (2004).
34. A. Avdeenkov and J. Bohn, Phys. Rev. A **66**, 052718 (2002).
35. G. C. Dousmanis, T. M. Sanders, Jr., and C. Townes, Phys. Rev. **100**, 1735 (1955).
36. H. E. Radford, Phys. Rev. **122**, 114 (1961).
37. J. ter Meulen and A. Dymanus, Astrophys. J. **172**, L21 (1972).
38. N. Kanekar, private communications (2006).